Preprints of the 21st IFAC World Congress (Virtual)
Berlin, Germany, July 12-17, 2020

# Robust Cascade LMI Design of MIMO Control System for Plasma Position, Current, and Shape Model with Time-Varying Parameters in a Tokamak

**Artem E. Konkov** * **Yuri V. Mitrishkin** ** **Pavel S. Korenev** ***
**Mikhail I. Patrov** ****

* *Faculty of Physics, Lomonosov Moscow State University, Institute of Control Sciences of Russian Academy of Sciences, Moscow, Russia (e-mail: konkov@physics.msu.ru).*
** *Faculty of Physics, Lomonosov Moscow State University, Institute of Control Sciences of RAS, Moscow, Russia (e-mail: yvm@mail.ru)*
*** *Institute of Control Sciences of RAS, Moscow, Russia (e-mail: pkorenev92@mail.ru)*
**** *Ioffe Institute of RAS, St. Petersburg, Russia (e-mail: michael.patrov@mail.ioffe.ru)*

**Abstract:** A new robust hierarchical plasma magnetic control system with time-varying parameters and cascade circuits for the Globus-M2 tokamak (Ioffe Institute) has been synthesized by means of the linear matrix inequalities (LMI) method. Each control cascade has a separate objective: placing poles of the closed-loop system in the $\mathbb{D}$-region to guarantee robust performance, restriction of the $\mathcal{H}_\infty$-norm of the transfer function between external disturbances and the plant outputs of the closed-loop system, tracking PF-currents, CS-current, plasma current, plasma position, gaps between the plasma separatrix and the first wall. Control cascades were synthesized for an array of plant linear models corresponding to reconstructed plasma equilibria at different time points of the tokamak discharges. The LMIs allow the synthesis of one LTI controller, providing the required performance and system stability margin *for each model from a given array.* Tracking cascades use new MIMO PID controllers adjusted by means of the LMIs.

*Keywords:* tokamak, plasma, LMI, robust control, MIMO PID, $\mathcal{H}_\infty$-control, $\mathbb{D}$-region

## 1. INTRODUCTION

The development of tokamaks (Wesson and Campbell, 2011) started in 1950s made them leading in the controlled thermonuclear fusion research. As tokamaks developed, plasma control systems were elaborated as tokamaks necessary components, without which the operation of modern tokamaks is impossible. The plasma control systems provide the tokamak performance, reliability, and survivability, as well as allow to reach their most economical regimes. Different approaches were used in magnetic control systems for plasma position, current, and shape: control channel decoupling, PID control, predictive model, $\mathcal{H}_\infty$ optimization theory, quadratic programming for saturation of control currents, adaptation of the plasma position to match the plasma shape, control with nonstationary controllers, hierarchical control, etc. See the survey Mitrishkin et al. (2018b,c).

Nevertheless, despite the fact that there is great progress in the development of plasma magnetic control systems they are far from complete for reliable use in future tokamak reactors like ITER and thermonuclear power plants (for instance in DEMO). In order to ensure their round-the-clock operation, the further elaboration is required with the applications of new structures of magnetic plasma control systems and new modern plasma control methods.

This work presents a new effective structure of plasma magnetic control system for the spherical Globus-M2 tokamak. The proposed control system makes use of two MIMO PID controllers in the cascades for plasma position, current and shape, and the second inner cascade for rejection of a multivariable external disturbance with a MIMO output controller. All controllers are designed with application of the LMI method which currently undergoes fast development in mathematical and numerical science and finds applications for plasma control in tokamaks. See e.g. Ariola et al. (2014); Pavlova et al. (2017); Konkov et al. (2018).

The LMI approach has essential advantages over other methods for the design of robust control systems. For instance in comparison with the $\mathcal{H}_\infty$ optimization theory the LMIs do not require using weighting functions like in the solutions of mixed sensitivity control problems (Skogestad and Postlethwaite, 2005), robust loop shaping

control (McFarlane and Glover, 1990) or fixed-structure $\mathcal{H}_\infty$ control (Apkarian et al., 2014). In applications of the Quantitative Feedback Theory (QFT) (Garcia-Sanz, 2017) one uses the boundaries caused by plant uncertainties in the Nichols amplitude-phase diagram to design the feedback and feedforward robust controllers by trial and error approach to meet the specifications at the set of predetermined frequencies, see Mitrishkin et al. (2018a, 2019). Instead of weighting functions $\mathbb{D}$-regions are used which are more obvious in the robust controller's design procedure. Moreover, the MIMO PID tuning method does not need decoupling of control channels and has the universal structure of statements of control problems.

The controlled plant and the transition to the LPV model in the state space form are described in Section 2. Section 3 presents cascades of the hierarchical control system. Sections 4 and 5 show the design of the cascades with the robust dynamic output-feedback controller and MIMO PID controllers. Section 6 gives the simulation results in Simulink of the designed control system.

## 2. PLASMA MODEL

The plant under control is the plasma in the Globus-M2 tokamak (Gusev et al., 2013), its output signals are as follows (37 outputs in total): vertical $Z$ and horizontal $R$ plasma positions, current in the central solenoid $I_{cs}$, 5 currents in the PF-coils

$$I_{pf} = \left[I_{pf\,1}\ I_{pf\,2}^{top}\ I_{pf\,2}^{bot}\ I_{pf\,3}\ I_{cc}\right]^{\mathrm{T}},$$

currents in vertical $I_{vfc}$ and horizontal $I_{hfc}$ field coils, plasma current $I_p$, poloidal magnetic flux $\Psi$ measured by 21 magnetic loops of the Globus-M2 tokamak, and 5 gaps between the separatrix and the first wall, see figure 1, $g = [g_1\ g_2\ g_3\ g_4\ g_5]^{\mathrm{T}}$.

The plasma models used for the controller synthesis are based on the Kirchhoff's law for currents in the tokamak, plasma motion equations, and the expression for gaps between the plasma and the first wall. The equations are linearized around the magnetohydrodynamic equilibria at various $t$-points of plasma discharge reconstructed from the tokamak's experimental data:

$$M(t)\delta\dot{I}+R_c\delta I+\frac{\partial\Psi_c}{\partial R}(t)\delta\dot{R}+\frac{\partial\Psi_c}{\partial Z}(t)\delta\dot{Z}+\frac{\partial\Psi_c}{\partial w}(t)\delta\dot{w}=\delta U,$$
$$\frac{\partial F_R}{\partial I}(t)\delta I+\frac{\partial F_R}{\partial R}(t)\delta R+\frac{\partial F_R}{\partial Z}(t)\delta Z+\frac{\partial F_R}{\partial w}(t)\delta w=0,$$
$$\frac{\partial F_Z}{\partial I}(t)\delta I+\frac{\partial F_Z}{\partial R}(t)\delta R+\frac{\partial F_Z}{\partial Z}(t)\delta Z+\frac{\partial F_Z}{\partial w}(t)\delta w=m\delta\ddot{Z},$$
$$\frac{\partial g}{\partial I}(t)\delta I+\frac{\partial g}{\partial R}(t)\delta R+\frac{\partial g}{\partial Z}(t)\delta Z+\frac{\partial g}{\partial w}(t)\delta w=\delta g,$$
$$\frac{\partial \Psi}{\partial I}(t)\delta I+\frac{\partial \Psi}{\partial R}(t)\delta R+\frac{\partial \Psi}{\partial Z}(t)\delta Z+\frac{\partial \Psi}{\partial w}(t)\delta w=\delta\Psi,$$
$$M(t)=\frac{\partial\Psi_c}{\partial I}(t),\ w=\begin{bmatrix}\beta_p\\ l_i\end{bmatrix}.$$

Here $I = [I_{hfc}, I_{vfc}, I_{cs}, I_{pf}^{\mathrm{T}}, I_v^{\mathrm{T}}, I_p]^{\mathrm{T}}$ is the vector of toroidal currents in the tokamak coils, the vacuum vessel, and the plasma, $U$ is the vector of the voltages applied to the coils, $\Psi_c$ is the vector of magnetic fluxes encircled by the currents, $M$ is the inductivity matrix, $R_c$ is the diagonal matrix of resistances in the circuits, $R, Z$ are horizontal and vertical coordinates of the plasma axis, $\beta_p$ and $l_i$ are the poloidal beta and the internal inductance of the plasma (Wesson and Campbell, 2011), $g$ is the vector of the gaps between the plasma separatrix and the first wall of the tokamak and $\Psi$ is the vector of poloidal magnetic fluxes measured by tokamak's magnetic loops. All variations depend on time.

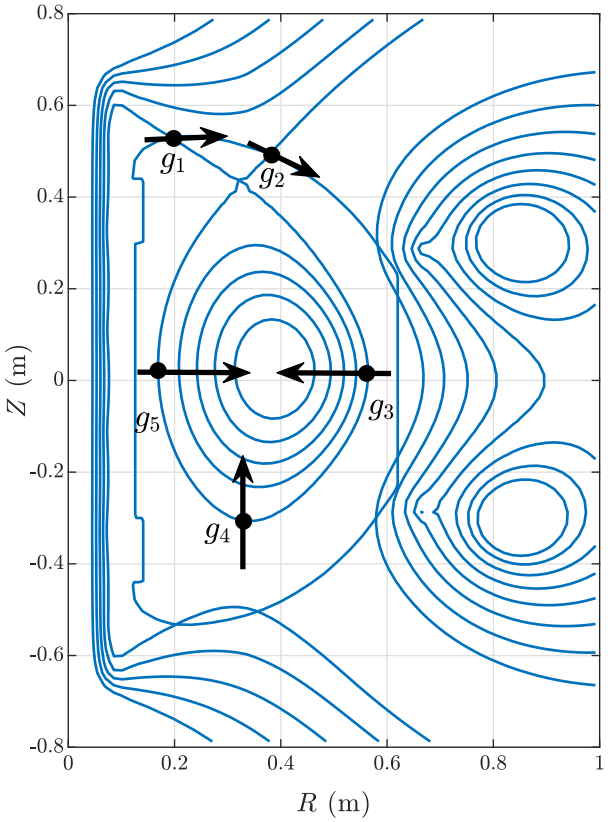


Fig. 1. Gaps between the separatrix and the first wall

Minor plasma disruptions are characterized by steep changes in $\beta_p$ and $l_i$, so the vector $\xi = \delta w$ may be considered as the disturbance vector.

Defining the state vector $x' = [\delta I^{\mathrm{T}}, \delta\dot{Z}, \delta Z]^{\mathrm{T}}$, the control vector $u = \delta U$ and the output vector

$$y = [\delta I_{hfc}, \delta I_{vfc}, \delta I_{cs}, \delta I_{pf}^{\mathrm{T}}, \delta I_p, \delta R, \delta Z, \delta g^{\mathrm{T}}, \delta\Psi^{\mathrm{T}}]^{\mathrm{T}},$$

the linear model can be expressed in the state-space form with time varying parameters:

$$\begin{cases} \dot{x}'(t) = A(t)x'(t) + B(t)u(t) + \\ \qquad + G'(t)\dot{\xi}(t) + E'(t)\xi(t), \\ y(t) = C(t)x'(t) + F'(t)\xi(t), \end{cases} \quad (1)$$

where

$$A(t) = -\tilde{M}^{-1}\begin{bmatrix} R_c\ \dfrac{\partial F_Z}{\partial I} - \dfrac{\partial F_Z}{\partial R}\dfrac{\partial F_R}{\partial I}\Big/\dfrac{\partial F_R}{\partial R} & 0 \\ 0 \qquad\qquad 0 & 0 \\ 0 \quad \dfrac{\partial F_Z}{\partial Z} - \dfrac{\partial F_Z}{\partial R}\dfrac{\partial F_R}{\partial Z}\Big/\dfrac{\partial F_R}{\partial R} & -1 \end{bmatrix}^{\mathrm{T}},$$

$$B(t)=\tilde{M}^{-1}\begin{bmatrix}1\\0\\0\end{bmatrix},\ G'(t)=-\tilde{M}^{-1}\begin{bmatrix}\dfrac{\partial\Psi_c}{\partial w} - \dfrac{\partial\Psi_c}{\partial R}\dfrac{\partial F_R}{\partial w}\Big/\dfrac{\partial F_R}{\partial R}\\ 0 \\ 0\end{bmatrix},$$

$$E'(t) = -\tilde{M}^{-1}\begin{bmatrix} 0 \\ \dfrac{\partial F_Z}{\partial w} - \dfrac{\partial F_Z}{\partial R}\dfrac{\partial F_R}{\partial w}\Big/\dfrac{\partial F_R}{\partial R} \\ 0 \end{bmatrix},$$

$$F'(t) = \begin{bmatrix} 0 \\ -\dfrac{\partial F_R}{\partial w}\Big/\dfrac{\partial F_R}{\partial R} \\ 0 \\ \dfrac{\partial g}{\partial w} - \dfrac{\partial g}{\partial R}\dfrac{\partial F_R}{\partial w}\Big/\dfrac{\partial F_R}{\partial R} \\ \dfrac{\partial \Psi}{\partial w} - \dfrac{\partial \Psi}{\partial R}\dfrac{\partial F_R}{\partial w}\Big/\dfrac{\partial F_R}{\partial R} \end{bmatrix},$$

$$\tilde{M}(t) = \begin{bmatrix} M - \dfrac{\partial \Psi_c}{\partial R}\dfrac{\partial F_R}{\partial I}\Big/\dfrac{\partial F_R}{\partial R} & 0 & \dfrac{\partial \Psi_c}{\partial Z} - \dfrac{\partial \Psi_c}{\partial R}\dfrac{\partial F_R}{\partial Z}\Big/\dfrac{\partial F_R}{\partial R} \\ 0 & m & 0 \\ 0 & 0 & 1 \end{bmatrix},$$

$$C(t) = \begin{bmatrix} 1 & 0 & 0 \\ -\dfrac{\partial F_R}{\partial I}\Big/\dfrac{\partial F_R}{\partial R} & 0 & -\dfrac{\partial F_R}{\partial Z}\Big/\dfrac{\partial F_R}{\partial R} \\ 0 & 0 & 1 \\ \dfrac{\partial g}{\partial I} - \dfrac{\partial g}{\partial R}\dfrac{\partial F_R}{\partial I}\Big/\dfrac{\partial F_R}{\partial R} & 0 & \dfrac{\partial g}{\partial Z} - \dfrac{\partial g}{\partial R}\dfrac{\partial F_R}{\partial Z}\Big/\dfrac{\partial F_R}{\partial R} \\ \dfrac{\partial \Psi}{\partial I} - \dfrac{\partial \Psi}{\partial R}\dfrac{\partial F_R}{\partial I}\Big/\dfrac{\partial F_R}{\partial R} & 0 & \dfrac{\partial \Psi}{\partial Z} - \dfrac{\partial \Psi}{\partial R}\dfrac{\partial F_R}{\partial Z}\Big/\dfrac{\partial F_R}{\partial R} \end{bmatrix}.$$

At the further variable transformation $x = x' - G'\xi$, $E = AG' + E' - \dot{G}'$, $F = CG' + F'$ in (1) the clear physical meaning of the state variables is lost, but a simpler, more suitable model for the controller design is obtained.
Control cascades are synthesized on an array of 50 models. The models correspond to the time points $t_1, \ldots, t_{50}$ from 175 to 200 ms (with 0.5 ms step) of the divertor phase of the discharge No. 37239 of the Globus-M2 tokamak. Denoting models in the array by the index $A_n = A(t_n), B_n = B(t_n)$, etc., $n = 1, \ldots, 50$, the resulting LTI model of the array with index n in new coordinates is written as follows:

$$\begin{cases} \dot{x}(t) = A_n x(t) + B_n u(t) + E_n \xi(t), \\ y(t) = C_n x(t) + F_n \xi(t), \end{cases} \tag{2}$$

where $x \in \mathbb{R}^{24}$, $u \in \mathbb{R}^8$, $y \in \mathbb{R}^{37}$, and $\xi \in \mathbb{R}^2$.

## 3. HIERARCHICAL CONTROL SYSTEM STRUCTURE

The block diagram of the hierarchical plasma control system is presented in figure 2; it contains four MIMO control cascades. Each cascade achieves its own control objective. The first cascade contains two current inverters and six rectifiers, they are actuators, see Kuznetsov et al. (2019); Mitrishkin et al. (2016). The second cascade with a robust dynamic output-feedback controller $K(s)$ is shown in figures 2 and 3 in blue. It has two objectives: it reduces the norm of the transfer function between the external disturbance $\xi$ and the outputs (currents $\delta I$, positions $\delta Z$, $\delta R$, and gaps $\delta g$), and places the poles of the closed-loop system in the $\mathbb{D}$-region. This is necessary to improve the performance of the control system: to reduce the oscillation index and transition time. This controller is synthesized for the entire array of models (2) describing plant dynamics at various time points of the discharge. That guarantees a proper margin of robust stability of the control system.

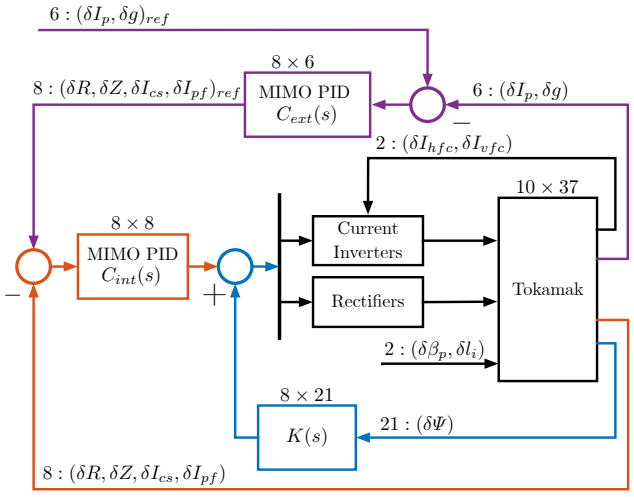


Fig. 2. Block diagram of plasma magnetic control system

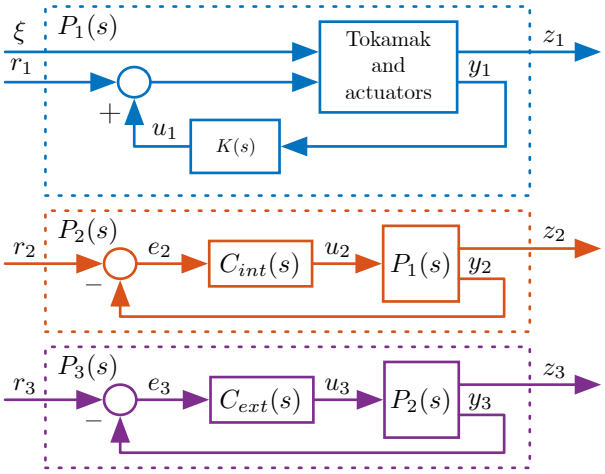


Fig. 3. Block diagrams of cascades of the control system

The third and fourth cascades shown in figures 2 and 3, red and purple, respectively, contain MIMO PID controllers with the same structure. The third cascade provides tracking of variations of plasma positions $\delta Z$, $\delta R$ and currents in the coils $\delta I_{cs}$, $\delta I_{pf}$ in line with the references. The fourth cascade provides tracking for variations of the plasma current $\delta I_p$ and the gaps $\delta g$; it generates references for the third cascade. Due to this, with the help of the fourth cascade, the control system provides *coordinated* control of gaps and plasma position on the one hand, and plasma current and currents in the coils on the other hand.

## 4. SYNTHESIS OF ROBUST DYNAMICAL OUTPUT-FEEDBACK CONTROLLER

The method is based on the Bounded Real Lemma and the generalized Lyapunov Theorem, see Duan and Yu (2013);

it is necessary to combine them into one LMI system. The approach used here for the output-feedback controller is based on Bakka and Karimi (2012). First, one needs to separate the plant outputs to $y_1 = \delta\Psi$ which are for feedback-loops outputs, and $z_1 = \begin{bmatrix}\delta Z & R & \delta I_{cs} & I\delta_{pf}^{\mathrm{T}} & \delta I_p & \delta g^{\mathrm{T}}\end{bmatrix}^{\mathrm{T}}$ which is the vector of interest, i.e. the purpose for $\mathcal{H}_\infty$-control:

$$\begin{cases}\dot{x} = Ax + Bu_1 + E\xi,\\ z_1 = C_1x + F_1\xi,\\ y_1 = C_2x + F_2\xi.\end{cases}$$

The controller is defined as

$$u_1(s) = K(s)y_1(s), \quad K(s)\begin{cases}\dot{\zeta} = A_k\zeta + B_ky_1,\\ u_1 = C_k\zeta + D_ky_1.\end{cases}$$

The closed-loop system shown in blue in figure 3 has the following form:

$$\begin{bmatrix}\dot{x}\\ \dot{\zeta}\end{bmatrix} = A_{cl}\begin{bmatrix}x\\ \zeta\end{bmatrix} + B_{cl}\xi, \quad z_1 = C_{cl}\begin{bmatrix}x\\ \zeta\end{bmatrix} + D_{cl}\xi,$$

$$\left[\begin{array}{c|c}A_{cl} & B_{cl}\\ \hline C_{cl} & D_{cl}\end{array}\right] = \left[\begin{array}{cc|c}A + BD_kC_2 & BC_k & E + BD_kF_2\\ B_kC_2 & A_k & B_kF_2\\ \hline C_1 & 0 & F_1\end{array}\right].$$

The Lyapunov matrix $\mathcal{P}$ must be represented as mutually inverse matrices

$$\mathcal{P} = \begin{bmatrix}Y & N\\ N^{\mathrm{T}} & \Omega_1\end{bmatrix}, \quad \mathcal{P}^{-1} = \begin{bmatrix}X & M\\ M^{\mathrm{T}} & \Omega_2\end{bmatrix},$$

where $\Omega_1$ and $\Omega_2$ are arbitrary matrices, see Scherer et al. (1997). Then the following notations are introduced

$$\hat{A} = NA_kM^{\mathrm{T}} + NB_kC_2X + YBC_kM^{\mathrm{T}} + \\ + Y\left(A + BD_kC_2\right)X,$$

$$\hat{B} = NB_k + YBD_k, \quad \hat{C} = C_kM^{\mathrm{T}} + D_kC_2X, \quad \hat{D} = D_k,$$

$$\Theta_1 = AX + B\hat{C} + \left(AX + B\hat{C}\right)^{\mathrm{T}}, \ \Theta_2 = \hat{A}^{\mathrm{T}} + A + B\hat{D}C_2,$$

$$\Theta_3 = YA + \hat{B}C_2 + \left(YA + \hat{B}C_2\right)^{\mathrm{T}}$$

to form the following LMI terms for $\mathcal{H}_\infty$-control and placement of the poles of a closed-loop system in $\mathbb{D}$-region:

$$\Sigma_1 = \begin{bmatrix}\Theta_1 & \Theta_2 & E + B\hat{D}F_2 & XC_1^{\mathrm{T}} + \hat{C}^{\mathrm{T}}F_2^{\mathrm{T}}\\ * & \Theta_3 & YE + \hat{B}F_2 & C_1^{\mathrm{T}} + C_2^{\mathrm{T}}\hat{D}^{\mathrm{T}}\\ * & * & -\gamma I & F_1^{\mathrm{T}}\\ * & * & * & -\gamma I\end{bmatrix},$$

$$\Sigma_2 = \begin{bmatrix}G_1 & H_1^{\mathrm{T}} & G_2 & H_2^{\mathrm{T}} & G_3 & H_3^{\mathrm{T}} & G_4 & H_4^{\mathrm{T}}\end{bmatrix},$$

$$\Sigma_3 = -\frac{1}{2}\mathrm{diag}\left(\epsilon_1^{-1}, \epsilon_1, \epsilon_1^{-1}, \epsilon_1, \epsilon_2^{-1}, \epsilon_2, \epsilon_2^{-1}, \epsilon_2\right),$$

$$\Sigma_4 = L_{\mathbb{D}} \otimes \begin{bmatrix}X & I\\ I & Y\end{bmatrix} + M_{\mathbb{D}} \otimes \begin{bmatrix}AX + B\hat{C} & A + B\hat{D}C\\ \hat{A} & YA + \hat{B}C\end{bmatrix} + \\ + M_{\mathbb{D}}^{\mathrm{T}} \otimes \begin{bmatrix}AX + B\hat{C} & A + B\hat{D}C\\ \hat{A} & YA + \hat{B}C\end{bmatrix}^{\mathrm{T}},$$

$$\Sigma_5 = \begin{bmatrix}\epsilon_1P_1 & N_1^{\mathrm{T}} & \epsilon_2P_2 & N_2^{\mathrm{T}} & \epsilon_3P_3 & N_3^{\mathrm{T}} & \epsilon_4P_4 & N_4^{\mathrm{T}}\end{bmatrix}$$

where $\epsilon_{1-4}$, $G_{1-4}$, $H_{1-4}$, $P_{1-4}$, and $N_{1-4}$ are obtained from the lemma in Khargonekar et al. (1990). $L_{\mathbb{D}}$ and $M_{\mathbb{D}}$ are the matrices of the characteristic function of the $\mathbb{D}$-region represented by the intersection of the circle with the center at the point $(0, 0)$ and the radius $r$, and the half-plane with the parameter $\alpha$, see Duan and Yu (2013),

$$\mathbb{D} = \{s \mid s \in \mathbb{C}^-, \ L_{\mathbb{D}} + sM_{\mathbb{D}} + \bar{s}M_{\mathbb{D}}^{\mathrm{T}} < 0\},$$

$$L_{\mathbb{D}} = \begin{bmatrix}2\alpha & 0 & 0\\ 0 & -r & 0\\ 0 & 0 & -r\end{bmatrix}, M_{\mathbb{D}} = \begin{bmatrix}1 & 0 & 0\\ 0 & 0 & 1\\ 0 & 0 & 0\end{bmatrix}.$$

Thus the final LMI system is formulated as follows

$$\begin{bmatrix}X & I\\ I & Y\end{bmatrix} \succeq 0, \begin{bmatrix}\Sigma_1 & \Sigma_2\\ \Sigma_2^{\mathrm{T}} & \Sigma_3\end{bmatrix} \preceq 0, \begin{bmatrix}\Sigma_4 & \Sigma_5\\ \Sigma_5^{\mathrm{T}} & \Sigma_3\end{bmatrix} \preceq 0.$$

The solution of this system *for all models from* (2) allows to obtain matrices $X$, $Y$, $\hat{A}$, $\hat{B}$, $\hat{C}$, and $\hat{D}$. After obtaining the matrices $M$ and $N$ from the factorization problem $MN^{\mathrm{T}} = I - XY$, one can determine the matrices of the controller

$$A_k = N^{-1}\Big(\hat{A} - NB_kC_2X - YBC_kM^{\mathrm{T}} - \\ - Y\left(A + BD_kC_2\right)X\Big)\left(M^{\mathrm{T}}\right)^{-1},$$

$$B_k = N^{-1}\left(\hat{B} - YBD_k\right),$$

$$C_k = \left(\hat{C} - D_kC_2X\right)\left(M^{\mathrm{T}}\right)^{-1}, \quad D_k = \hat{D}.$$

## 5. MIMO PID CONTROLLER DESIGN

The method in Boyd et al. (2016) allows synthesizing the MIMO tracking control system with a new type of controllers. The MIMO PID controller is used in the third and fourth cascades, shown in figures 2 and 3 in red and purple. The MIMO PID controller is defined as

$$u(s) = C(s)e(s), \quad C(s) = K_P + \frac{1}{s}K_I + \frac{s}{\tau s + 1}K_D,$$

where $u(s) \in \mathbb{C}^m$ is the Laplace transform of the plant inputs vector, $e(s) \in \mathbb{C}^q$ is the error between the references $r(s)$ and the outputs $y(s)$ of the plant. The PID coefficients are non-diagonal matrices

$$K_P \in \mathbb{R}^{m\times q}, \quad K_P \in \mathbb{R}^{m\times q}, \quad K_P \in \mathbb{R}^{m\times q}.$$

The following closed-loop responses and matrix transfer functions will be used for the design of controllers:

$$e(s) = S(s)r(s), \quad S(s) = \left(I + P(s)C(s)\right)^{-1},$$

$$y(s) = T(s)r(s), \quad T(s) = P(s)C(s)\left(I + P(s)C(s)\right)^{-1},$$

$$u(s) = Q(s)r(s), \quad Q(s) = C(s)\left(I + P(s)C(s)\right)^{-1}.$$

The matrix $(P(0)K_I)^{-1}$ is the matrix of the static and low-frequency sensitivity; it is defined as

$$\left.\frac{dS}{ds}\right|_{s=0} = \left(P(0)K_I\right)^{-1}, \ S(s) \approx s\left(P(0)K_I\right)^{-1} \text{for small } |s|,$$

the Q-parameter is necessary for control restrictions, it is caused by engineering constraints of the actuators.

Now it is possible to formulate the problem of the synthesis of the MIMO PID controller as an SDP problem. Next, the transition is done from the transfer functions to the matrix values of the transfer functions at the selected frequencies, and, accordingly, from the $\mathcal{H}_\infty$-norms of the

matrix transfer functions to the spectral norms of the numerical matrices:

$$\begin{cases} \min & \|(P(0)K_I)^{-1}\|_2, \\ \text{s.t.} & \|S(s)\|_\infty \le S_{\max}, \\ & \|T(s)\|_\infty \le T_{\max}, \\ & \|Q(s)\|_\infty \le Q_{\max}. \end{cases} \longrightarrow \begin{cases} \min & \|(P(0)K_I)^{-1}\|_2, \\ \text{s.t.} & \|S_k\|_2 \le S_{\max}, \\ & \|T_k\|_2 \le T_{\max}, \\ & \|Q_k\|_2 \le Q_{\max}. \end{cases}$$

where $k = 1, \dots, N$, $P_k = P(j\omega_k)$, $\omega_k \in [\omega_1, \dots, \omega_N]$,

$$C_k = K_P + \frac{1}{j\omega_k} K_I + \frac{j\omega_k}{\tau j\omega_k + 1} K_D. \tag{3}$$

The transition ($\longrightarrow$) from the transfer functions to the values of these transfer functions at the selected frequencies is the main idea of the method; it allows to reduce the problem to the matrix inequalities form

$$\begin{cases} \max & \mu, \\ \text{s.t.} & (P(0)K_I)^{\mathrm{H}}(P(0)K_I) \succeq \mu^2 I, \\ & (I + P_kC_k)^{\mathrm{H}}(I + P_kC_k) \succeq (1/S_{\max}^2) I, \\ & (I + P_kC_k)^{\mathrm{H}}(I + P_kC_k) \succeq \\ & \qquad \succeq (1/T_{\max}^2)(P_kC_k)^{\mathrm{H}}(P_kC_k), \\ & (I + P_kC_k)^{\mathrm{H}}(I + P_kC_k) \succeq (1/Q_{\max}^2) C_k^{\mathrm{H}} C_k. \end{cases} \tag{4}$$

This system of matrix inequalities contains three unknown matrices $K_P$, $K_I$, and $K_D$ included in $C_k$ in (3), and the target $\mu$. The matrix inequalities in system (4) are not linear with respect to the unknown matrices of the controller; moreover, the left-hand sides of the inequalities are not convex. To obtain a solution for (4), it must be reduced to the LMI system by means of a convex-concave procedure, described in detail in Lipp and Boyd (2015). The solution of the original system (4) is found by iteratively solving the equivalent LMI system, approaching the optimal value of $\mu_{max}$ at each iteration.

The following signals were used in the synthesis of cascades $P_2(s)$ and $P_3(s)$, see figure 3: $u_3(s) = r_2(s)$, $u_2(s) = r_1(s)$, $z_2$ and $z_3$ are vectors with other signals of the plant, $r_2(s)$ and $r_3(s)$ are references for outputs

$$y_2(s) = \begin{bmatrix} \delta R \\ \delta Z \\ \delta I_{cs} \\ \delta I_{pf} \end{bmatrix} \in \mathbb{C}^8, \quad y_3(s) = \begin{bmatrix} \delta I_p \\ \delta g \end{bmatrix} \in \mathbb{C}^6.$$

Sensitivity functions of these cascades are

$$e_2(s) = S_2(s) r_2(s), \quad S_2(s) = \Big(I + P_1(s) C_{int}(s)\Big)^{-1},$$
$$e_3(s) = S_3(s) r_3(s), \quad S_3(s) = \Big(I + P_2(s) C_{ext}(s)\Big)^{-1}.$$

The transfer functions $T(s)$ and $Q(s)$ for these cascades are obtained similarly. System (4) is solved with parameters $S_{\max}$, $T_{\max}$, $Q_{\max}$, $N$, and $\tau$ for each cascade, *while there is one solution for all models from* (2). Thus, matrix inequalities in (4) are sequentially solved first for $C_{int} \in \mathbb{C}^{8\times 8}$, and then for $C_{ext} \in \mathbb{C}^{8\times 6}$, see them in figure 3.

## 6. SIMULATION RESULTS

The LMIs for the control design are solved using CVX with SDPT3 4.0 solver interfaced with MATLAB, see CVX Research (2012); Grant and Boyd (2008). The simulation was carried out in Simulink using an LPV block for the plant model, models switching starts from 175 ms. The results are presented in figure 4, which contains variations of gaps $\delta g_{1-5}$, plasma current $\delta I_p$, poloidal beta $\delta\beta_p$, and internal

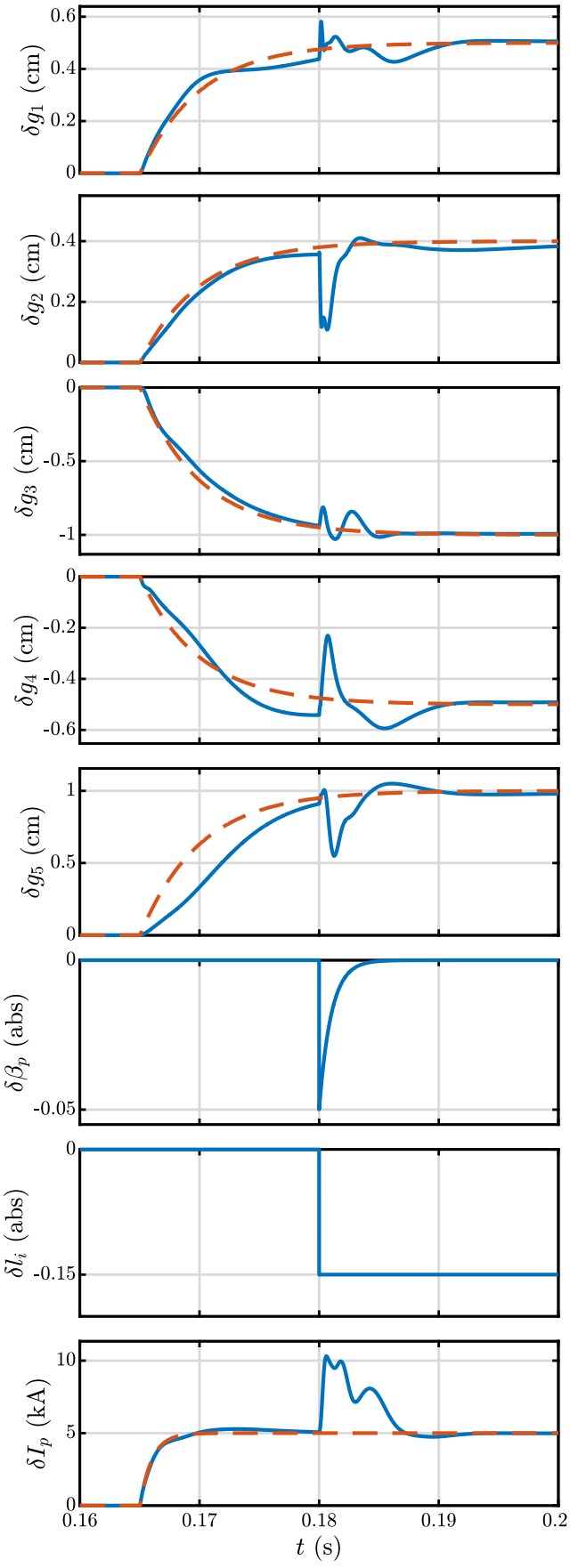


Fig. 4. The simulation results of the control system of the plasma for discharge No. 37239 when minor disruption occur. Red lines are references.

plasma inductance $\delta l_i$ when the minor disruption occurs, and the control system moving the separatrix to a new location. The following parameters were used: for second cascade $\gamma = 10^2$, $\alpha = 10^3$, $r = 5 \cdot 10^4$; for third cascade $S_{\max} = 1.6$, $T_{\max} = 1.8$, $Q_{\max} = 5/\sigma_{\min}\big(P(0)\big)$; for fourth cascade $S_{\max} = 1.2$, $T_{\max} = 1.4$, $Q_{\max} = 10/\sigma_{\min}\big(P(0)\big)$.

## 7. CONCLUSION

The new robust control systems have been designed for dynamic plants with variable parameters and applied in modelling to the plasma in the spherical tokamak Globus-M2. Robust control systems were synthesized by the LMI method *for the array of linear plasma models* with time-invariant parameters. That made it possible to apply the transfer function and frequency response methods to each model. Then the time-varying plasma models were obtained by the Simulink LPV block in simulations.

## ACKNOWLEDGEMENTS

The reported research was funded by Russian Foundation for Basic Research, project No 19-31-90136, and Russian Science Foundation, project No 17-19-01022.

## REFERENCES

Apkarian, P., Gahinet, P., and Buhr, C. (2014). Multi-model, multi-objective tuning of fixed-structure controllers. In *2014 European Control Conference (ECC)*, 856–861.

Ariola, M., Tommasi, G.D., Pironti, A., and Villone, F. (2014). Control of resistive wall modes in tokamak plasmas. *Control Engineering Practice*, 24, 15 – 24. doi: 10.1016/j.conengprac.2013.11.009.

Bakka, T. and Karimi, H.R. (2012). Robust $\mathcal{H}_\infty$ dynamic output feedback control synthesis with pole placement constraints for offshore wind turbine systems. *Mathematical Problems in Engineering*, 2012, 18.

Boyd, S., Hast, M., and Åström, K.J. (2016). MIMO PID tuning via iterated LMI restriction. *International Journal of Robust and Nonlinear Control*, 26(8), 1718–1731. doi:10.1002/rnc.3376.

CVX Research, I. (2012). CVX: Matlab software for Disciplined Convex Programming, version 2.0. URL `http://cvxr.com/cvx`.

Duan, G. and Yu, H. (2013). *LMIs in Control Systems*. CRC Press, Taylor & Francis Group.

Garcia-Sanz, M. (2017). *Robust Control Engineering. Practical QFT Solutions*. Boca Raton: CRC Press, Taylor & Francis Group.

Grant, M. and Boyd, S. (2008). Graph implementations for nonsmooth convex programs. In V. Blondel, S. Boyd, and H. Kimura (eds.), *Recent Advances in Learning and Control*, Lecture Notes in Control and Information Sciences, 95–110. Springer-Verlag Limited.

Gusev, V., Azizov, E., Alekseev, A., and et al. (2013). Globus-M results as the basis for a compact spherical tokamak with enhanced parameters Globus-M2. *Nuclear Fusion*, 53(9), 093013. doi:10.1088/0029-5515/53/9/093013.

Khargonekar, P.P., Petersen, I.R., and Zhou, K. (1990). Robust stabilization of uncertain linear systems: quadratic stabilizability and $\mathcal{H}_\infty$ control theory. *IEEE Transactions on Automatic Control*, 35(3), 356–361. doi: 10.1109/9.50357.

Konkov, A.E., Mitrishkin, Y.V., and Kartsev, N.M. (2018). Synthesis of the outer cascade for plasma magnetic control in the Globus-M tokamak by using linear matrix inequalities method. In *2018 14th International Conference "Stability and Oscillations of Nonlinear Control Systems" (Pyatnitskiy's Conference) (STAB)*, 1–4. doi:10.1109/STAB.2018.8408367.

Kuznetsov, E.A., Mitrishkin, Y.V., and Kartsev, N.M. (2019). Current inverter as self-oscillating actuator in applications for plasma position control systems in the Globus-M/M2 and T-11M tokamaks. *Fusion Engineering and Design*, 143, 247–258.

Lipp, T. and Boyd, S. (2015). Variations and extension of the convex–concave procedure. *Optimization and Engineering*, 17(2), 263–287. doi:10.1007/s11081-015-9294-x.

McFarlane, D.C. and Glover, K. (eds.) (1990). *Robust Controller Design Using Normalized Coprime Factor Plant Descriptions*. Springer-Verlag. doi:10.1007/bfb0043199.

Mitrishkin, Y.V., Pavlova, E.A., Kuznetsov, E.A., and Gaydamaka, K.I. (2016). Continuous, saturation, and discontinuous tokamak plasma vertical position control systems. *Fusion Engineering and Design*, 108, 35–47. doi:10.1016/j.fusengdes.2016.04.026.

Mitrishkin, Y.V., Prokhorov, A.A., Korenev, P.S., and Patrov, M.I. (2018a). Robust plasma position, current, and shape control system simulated on plasma evolution code for the spherical tokamak Globus-M. In *Proceedings of the 45th European Physical Society Conference on Plasma Physics*, P4.1079. EPS, Prague, Czech Republic.

Mitrishkin, Y., Korenev, P., Prokhorov, A., Kartsev, N., and Patrov, M. (2018b). Plasma control in tokamaks. Part 1. Controlled thermonuclear fusion problem. Tokamaks. Components of control systems. *Advances in Systems Science and Applications*, 18(2), 26–52.

Mitrishkin, Y.V., Kartsev, N.M., Pavlova, E.A., Prohorov, A.A., Korenev, P.S., and Patrov, M.I. (2018c). Plasma control in tokamaks. Part 2. Magnetic plasma control systems. *Advances in Systems Science and Applications*, 18(3), 39–78.

Mitrishkin, Y., Prokhorov, A., Korenev, P., and Patrov, M. (2019). Hierarchical robust switching control method with the improved moving filaments equilibrium reconstruction code in the feedback for tokamak plasma shape. *Fusion Engineering and Design*, 138, 138–150. doi:10.1016/j.fusengdes.2018.10.031.

Pavlova, E.A., Mitrishkin, Y.V., and Khlebnikov, M.V. (2017). Control system design for plasma unstable vertical position in a tokamak by linear matrix inequalities. In *2017 IEEE 11th International Conference on Application of Information and Communication Technologies (AICT)*, 1–5. doi:10.1109/ICAICT.2017.8687042.

Scherer, C., Gahinet, P., and Chilali, M. (1997). Multiobjective output-feedback control via LMI optimization. *IEEE Transactions on Automatic Control*, 42(7), 896–911. doi:10.1109/9.599969.

Skogestad, S. and Postlethwaite, I. (2005). *Multivariable Feedback Control: Analysis and Design*. J. Wiley & sons.

Wesson, J. and Campbell, D. (2011). *Tokamaks*. International Series of Monographs on Physics. OUP Oxford.